32nd Annual International Conference of the IEEE EMBS
Buenos Aires, Argentina, August 31 - September 4, 2010

Estimated Venous Return Surface and Cardiac Output Curve Precisely Predicts New Hemodynamics after Volume Change

Masaru Sugimachi, *Member, IEEE*, Kenji Sunagawa, *Member, IEEE*,
Kazunori Uemura, Atsunori Kamiya, Shuji Shimizu, Masashi Inagaki and Toshiaki Shishido

Abstract— **In our extended Guyton's model, the ability of heart to pump blood is characterized by a cardiac output curve and the ability of vasculature to pool blood by a venous return surface. These intersect in a three-dimensional coordinate system at the operating right atrial pressure, left atrial pressure, and cardiac output. The baseline cardiac output curve and venous return surface and their changes after volume change would predict new hemodynamics. The invasive methods needed to precisely characterize cardiac output curve and venous return surface led us to aim at estimating cardiac output curve and venous return surface from a single hemodynamic measurement. Using the average values for two logarithmic function parameters, and for two slopes of a surface, we were able to estimate cardiac output curve and venous return surface. The estimated curve and surface predicted new hemodynamics after volume change precisely.**

I. Introduction

OUR group has developed an extended Guyton's cardiovascular model, where the ability of the right- and left-sided heart to pump blood is integratively characterized by a single curve (cardiac output curve) and the ability of vasculature to pool blood is expressed as a surface (venous return surface). The cardiac output curve and the venous return surface intersect in a three-dimensional coordinate system, and the three coordinates show the operating right atrial pressure (RAP), left atrial pressure (LAP), and cardiac output (CO), respectively (Fig. 1).

If one knows the baseline cardiac output curve and venous return surface and how these change after volume infusion and depletion, one can predict new hemodynamics by combining a new cardiac output curve and a new venous return surface. The precise characterization of cardiac output curve and venous return surface, however, needs extremely invasive measures for changing loading conditions to be applicable to patients with heart diseases (see Sections IIB and IIC for the detailed invasive methods used in animal experiments). Therefore, the aim of this study was to circumvent this difficulty by establishing a method to approximately obtain the cardiac output curve and venous return surface from a single hemodynamic measurement.

Manuscript received April 7, 2009. This work was supported in part by Grant-in-Aid for Scientific Research (B 20300164, C 20500404) from the Ministry of Education, Culture, Sports, Science and Technology, by Health and Labour Sciences Research Grants (H20-katsudo-shitei-007) from the Ministry of Health Labour and Welfare of Japan.

M. Sugimachi, K. Uemura, A. Kamiya, S. Shimizu, M. Inagaki and T. Shishido are with the National Cardiovascular Center Research Institute, Suita, Osaka 5658565, Japan (corresponding author Masaru Sugimachi to provide phone: +81-6-6833-5012; fax: +81-6-6835-5403; e-mail: su91mach@ri.ncvc.go.jp).

K. Sunagawa is with Kyushu University, Fukuoka 8128582 Japan. (e-mail: sunagawa@cardiol.med.kyushu-u.ac.jp).

II. Model and Methods

A. Extended Guyton's Model

We have extended Guyton's model [1] to handle a number of difficulties frequently encountered in clinical settings in patients with predominantly unilateral heart failure.

First, we extended a 2D (RAP-CO) Guyton's model to a 3D (RAP-LAP-CO) model, and introduced a third axis for LAP (Fig. 1) [2], [3]. By this modification, we can get the operating LAP directly from the intersection between cardiac output curve and venous return surface. LAP indicates the degree of pulmonary congestion and inadequate blood oxygenation, and normal range of LAP is as important as that of cardiac output and that of blood pressure for sustaining life.

Second, in this 3D model, we can separately express the changes in pumping ability of the right- and left-sided heart; the 3D cardiac output curve (Fig. 1, thick curve) is, in reality, the integration of two separate 2D cardiac output curves. The pumping ability of the right-sided heart can be obtained by projecting the 3D curve to the RAP-CO plane, and that of the

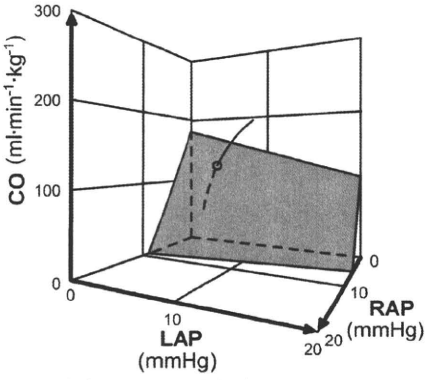

Fig. 1. An extended Guyton's model. The curve integratively expresses the pumping ability of right- and left-sided heart. The shaded surface characterizes the blood-pooling ability of the vasculature. RAP, right atrial pressure; LAP, left atrial pressure; CO, cardiac output (per kg of body weight).

left-sided heart can be obtained by projecting it to the LAP-CO plane. The preferential decrease in the pumping ability of the left-sided heart, such as seen in the ischemic heart disease, would rotate the projected curve to the RAP-LAP plane to the direction of LAP axis.

Third, the blood-pooling ability of the vasculature and the effect of stressed blood on the vasculature can be expressed by the venous return surface (Fig. 1, shaded surface). This surface remains the same so long as the total stressed volume is unchanged irrespective of its distribution. Increased LAP and pulmonary congestion associated with left-sided heart failure is characterized by blood redistribution from systemic to pulmonary vascular beds. Blood redistribution, however, would not change the venous return surface itself (i.e., unaffected by the changes in pumping ability). This is in sharp contrast with the classical venous return curve of Guyton's model. The relatively flat slope of the surface to the direction of LAP axis indicates the smaller blood-pooling ability of pulmonary vascular beds. As a result, the decrease in RAP with systemic-to-pulmonary blood redistribution is much smaller than the increase in LAP. This is shown, also illustratively in Fig. 1, by moving along the venous return surface and parallel to the RAP-LAP plane (keeping CO constant).

B. Animal Experiments to Characterize Cardiac Output Curve

We planned to characterize both cardiac output curve and venous return surface as precisely as possible in animals by using even the most invasive methods. In characterizing the pumping ability, only the heart of animals is needed; in characterizing the blood-pooling ability, only the vasculature of animals is needed.

The experiment for the characterization of cardiac output curve was less invasive. We do not need to physically detach the vasculature from the heart. Rather, in 7 dogs, by withdrawing and transfusing blood in a stepwise manner, we were able to obtain both right- and left-sided cardiac output curve simultaneously.

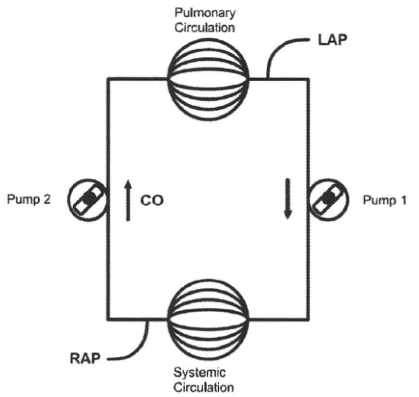

Fig. 2. An experimental scheme to characterize venous return surface. By replacing the right- and the left-sided heart with respective roller pumps, one can change cardiac output of the right- and the left-sided heart independently.

C. Animal Experiments to Characterize Venous Return Surface

Figure 2 depicts the scheme of an experiment to characterize the venous return surface. To extract only the vasculature and to physically remove the animal heart from the cardiovascular system, we replaced the right- and the left-sided heart with respective roller pumps. These pumps allow us to change CO of the right- and left-sided heart independently. Changing the flow of the two pumps at the same level would simulate the weak or strong heart. Transient unbalancing flow would redistribute blood between systemic and pulmonary vascular beds.

In each of 6 canine preparations, we obtained 6 different hemodynamic (CO, RAP, LAP) data sets. In each animal, these sets of data were fit to a flat surface in 3D coordinate system by linear regression analysis. CO was selected as a dependent variable and RAP (~2-5 mmHg) and LAP (~0-10 mmHg) are selected as independent variables.

D. Method to Estimate Cardiac Output Curve from a Single Hemodynamic Data Set

We fit experimental data to two logarithmic curves (one for the right- and the other for the left-sided heart), based on the knowledge of exponential end-diastolic pressure volume relationship and linear end-systolic pressure volume relationship, as follows.

$$CO = S\,[\ln(P - A) + B]$$

Here, P indicates RAP or LAP; A, B, and S are parameters. As analytical solution indicated that A and B is only dependent on diastolic properties of the ventricles, and is unlikely to change acutely, we fixed these parameters as their respective average values. This enabled one to estimate cardiac output curve from a single hemodynamic data set.

E. Method to Estimate Venous Return Surface from a Single Hemodynamic Data Set

We were able to fit experimental data to a flat surface well (r^2=0.92 to 0.99). As the surfaces from 6 animals were reasonably parallel (see Results), we used average slopes to estimate venous return surface from a single hemodynamic data set. Furthermore, as CO-axis intercept was linearly related to the withdrawn or transfused blood volume, we used this relationship to estimate a new venous return surface after blood volume change.

III. Results

A. Method to Estimate Cardiac Output Curve from a Single Hemodynamic Data Set

We were able to fit the cardiac output curve of both the right- and the left-sided heart by logarithmic functions (right-sided heart, r^2=0.90 to 0.99; left-sided heart, r^2=0.95 to 0.99). Since standard deviation of parameter A (1.29) or that of parameter

B (1.25) was much smaller than that of parameter S (30.9), we used the respective average values for A and B. The obtained cardiac output curves for right- and left-sided heart were as follows.

$$CO = S_R [\ln(RAP - 2.13) + 1.90] \quad (1)$$

$$CO = S_L [\ln(LAP - 2.03) + 0.80] \quad (2)$$

Parameters S_R and S_L can be used to represent the magnitude of the pumping ability of the right- and left-sided heart, respectively. As S_R and S_L can be calculated from a single set of hemodynamic data, we can approximately get cardiac output curve.

B. Method to Estimate Cardiac Output Curve from a Single Hemodynamic Data Set

In Figure 3 we have shown the venous return surfaces obtained from all 6 dogs. The surfaces were shown (as if they were lines) from the direction parallel to the surface. The figure indicates that in each of 6 dogs, all 6 data sets are located very near the flat surface. This implied the goodness of the fit of these data points to the flat surface. It is also shown that three coordinate axes are almost parallel among these dogs. This is because the slopes of the surface were almost the same among animals. These experimental results indicated that the venous return surface is linear and can be expressed by a common equation for all animals.

$$CO = CO_{max} - 19.61\ RAP - 3.49\ LAP.$$

Further, by infusing or withdrawing known amounts of blood, we were able to relate CO_{max} to blood volume as

$$CO_{max} = V / 0.129 \quad (3)$$

where V is total intravascular stressed blood volume. Combining these equations resulted in

$$CO = V / 0.129 - 19.61\ RAP - 3.49\ LAP. \quad (4)$$

Parameter V can be used to monitor the changes in total stressed blood volume. As V can be calculated from a single set of hemodynamic data, we can approximately get venous return surface.

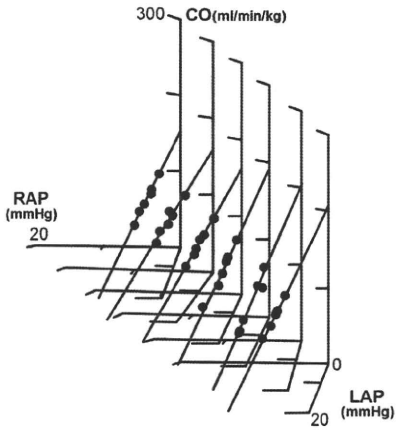

Fig. 3. Venous return surfaces obtained from 6 dogs. For each dog, the venous return surface was projected in a direction parallel to the surface, and was superimposed with each other.

C. Prediction of New Hemodynamics after Volume Change

We predicted new hemodynamics after volume change as follows. First, baseline cardiac output curve (Equations 1 and 2) and venous return surface (Equation 4) were approximately estimated from a single baseline hemodynamic data, by the methods shown in two previous sections IIIA and IIIB. Next, a new venous return surface was estimated by changing CO_{max} according to Equation 3. We assumed that cardiac output curve would not change by the volume change. Finally, new hemodynamics data were estimated by calculating the intersection between cardiac output curve and venous return surface.

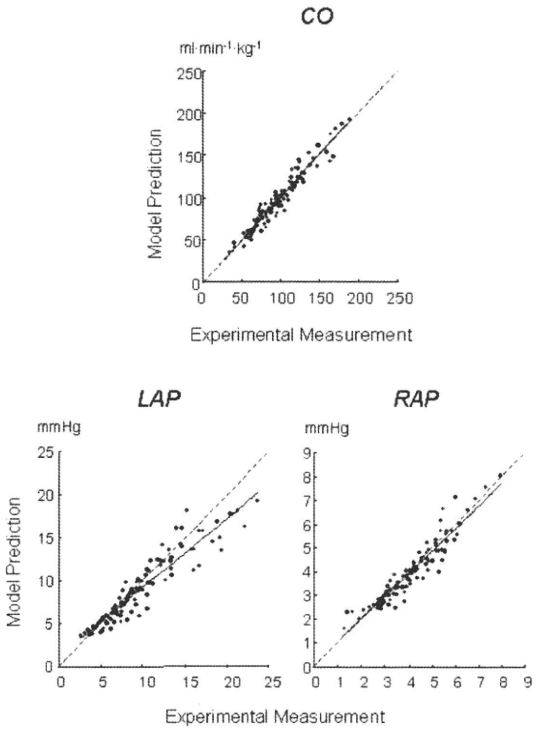

Fig. 4. Prediction of CO, LAP, and RAP from estimated cardiac output curve and venous return surface after volume change.

Using these new estimated cardiac output curve and venous return surface, we were able to predict the hemodynamics (y value) after withdrawal or transfusion of blood of known volume precisely as compared to actually measured (x value) (CO: $y = 0.93x + 6.5$, $r^2 = 0.96$, SEE [standard error of estimate] = 7.5 $ml \cdot min^{-1} \cdot kg^{-1}$; LAP: $y = 0.90x + 0.5$, $r^2 = 0.93$, SEE = 1.4 mmHg; RAP: $y = 0.87x + 0.4$, $r^2 = 0.91$, SEE = 0.4 mmHg) (Fig. 4) [3].

IV. Discussion

A. Most Undiagnosed Property: Total Stressed Blood Volume

The three major players of the cardiovascular system are heart

(pumps), vasculature (tubes with resistive and capacitive function), and blood. These three components interactively determine all hemodynamic variables. Of these, pump function and resistive function of vasculature have been repeatedly evaluated in previous studies. These properties were also evaluated clinically.

In contrast, evaluation of the vascular capacitive function and that of the blood volume have been relatively ignored. Even though blood volume drastically changes, there have been no reasonable methods to evaluate total stressed blood volume precisely. Simple measurement of central venous pressure (i.e., RAP) cannot be a proxy marker of blood volume, as this pressure value also changes with pump function or with redistribution of blood.

It is clear from our results [$V = (CO + 19.61\ RAP + 3.49\ LAP) \times 0.129$] that blood volume (V) is not solely determined by RAP. Rather, all three variables CO, RAP and LAP contribute (not as differently as have been considered) to the changes in blood volume. Clinicians should know that when LAP increases by 5.6 mmHg, or CO increases by 0.98L/min in 50-Kg patients, similar blood volume increases as RAP is increased by 1 mmHg.

Implantable devices with volume monitoring functionality for patients with heart failure should also take these results into consideration.

B. Hemodynamic Variables and Cardiovascular Properties

In clinical practice, physicians have to restore hemodynamic variables to their respective normal range. Of these, the most important three variables include blood pressure, CO and LAP. These variables are essentially important as blood pressure determines the perfusion of vital organs (for short-term need), CO determines the perfusion of peripheral tissues (for long-term need), and LAP determines blood oxygenation in lungs.

These hemodynamic variables are, in turn, determined by the interaction between cardiovascular properties, such as pump, resistance, capacitance, and blood volume. What clinicians should know, monitor, and correct are in reality these cardiovascular properties. Most drugs and interventions are aimed at correcting mainly one of these properties. From these viewpoints, the method to continuously estimate cardiovascular properties from measured hemodynamics is the most basic need in patient monitoring.

V. Conclusion

We have successfully developed a method to estimate the cardiac output curve and venous return surface from a single hemodynamic data set. This method enabled to predict new hemodynamics after withdrawal or transfusion of blood of known volume.

References

[1] A. C. Guyton, "Determination of cardiac output by equating venous return curves with cardiac response curves," *Physiol. Rev.* vol. 35, no. 1,123–129, Jan. 1955.

[2] K. Uemura, M. Sugimachi, T. Kawada, A. Kamiya, Y. Jin, *et al.*, "A novel framework of circulatory equilibrium," *Am. J. Physiol. Heart Circ. Physiol.* vol. 286, no. 6, pp. H2376–H2385, Jun. 2004.

[3] K. Uemura, T. Kawada, A. Kamiya, T. Aiba, I. Hidaka, *et al.*, "Prediction of circulatory equilibrium in response to changes in stressed blood volume," *Am. J. Physiol. Heart Circ. Physiol.* vol. 289, no. 1, H301–H307, Jul. 2005.

32nd Annual International Conference of the IEEE EMBS
Buenos Aires, Argentina, August 31 - September 4, 2010

Development of artificial bionic baroreflex system

Kenji Sunagawa, *Senior Member, IEEE* and Masaru Sugimachi, *Member, IEEE*

Abstract—**The baroreflex system is the fastest mechanism in the body to regulate arterial pressure. Because the neural system (i.e., autonomic nervous system) mediates the baroreflex and the system operates under the closed-loop condition, the quantitative dynamic characteristics of the baroreflex system remained unknown until recently despite the fact that a countless number of observational and qualitative studies had been conducted. In order to develop the artificial baroreflex system, i.e., the bionic baroreflex system, we first anatomically isolated the carotid sinuses to open the baroreflex loop and identified the open-loop transfer function of the baroreflex system using white noise pressure perturbations. We found that the baroreflex system is basically a lowpass filter and remarkably linear. As an actuator to implement the bionic baroreflex system, we then stimulated the sympathetic efferent nerves at various parts of the baroreflex loop and identified the transfer functions from the stimulation sites to systemic arterial pressure. We found that the actuator responses can be described remarkably well with linear transfer functions. Since transfer functions of the native baroreflex and of the actuator were identified, the controller that is required to reproduce the native baroreflex transfer function can be easily derived from those transfer functions. To examine the performance of bionic baroreflex system, we implemented it animal models of baroreflex failure. The bionic baroreflex system restored normal arterial pressure regulation against orthostatic stresses that is indistinguishable from the native baroreflex system.**

I. Introduction

Baroreflex is known to be the fastest mechanism in the body to stabilize arterial pressure. The reflex makes use of negative feedback mechanism. The baroreceptors sitting in the arterial wall sense arterial pressure and send the pressure signal to the brainstem through the afferent nerve fibers. The brainstem receives the pressure signal and judges the level of arterial pressure. If the level is low, the brainstem activates the sympathetic system innervating the heart and vascular system to increase arterial pressure. If the level of arterial pressure is high, the brainstem withdraws the sympathetic activation.

The baroreflex system is critically important in animal, particularly in human. This is because, unlike animals with four legs, the position dependent gravitational effect on circulation is most prominent in human. It is well known that once we lose the normal function of baroreflex, we no longer keep sitting and/or standing positions because of position induced profound hypotension and hypoperfusion of the brain. Baroreflex failure destroys normal life and is a devastating pathological state in human. However, since the baroreflex failure is a disease of the neural system, no effective treatment has ever developed to save those patients.

Baroreflex failure could happen under various conditions. In some patients, they lost baroreflex function because they have problems in the baroreceptors, the brainstem and/or the spinal cord. In those patients, if we can develop a mechanism to activate their sympathetic efferent system in response to changes in arterial pressure just like the native brainstem does, in theory, normal baroreflex function can be restored.

The purpose of this investigation is to develop an artificial baroreflex system, so called the bionic baroreflex system, to restore normal baroreflex function to overcome such a serious pathological condition.

II. Bionic Baroreflex System

Shown in Fig. 1 are how we identify the transfer function of the controller of bionic baroreflex system. First we identify the transfer function of the baroreflex open loop (H_{NATIVE}) from baroreceptor pressure to arterial pressure responses. We then electrically stimulate a particular site in the baroreflex loop and identify the transfer function of the actuator from the stimulation to arterial pressure responses ($H_{STM \rightarrow AOP}$). Since the controller will be in series with the actuator, the transfer function of bionic baroreflex system becomes identical to the native baroreflex system when the transfer function of controller (H_{BIONIC}) satisfies the following equation:

$$H_{NATIVE} = H_{BIONIC} \times H_{STM \rightarrow AOP}$$

In theory both H_{NATIVE} and $H_{STM \rightarrow AOP}$ can be experimentally determined. Therefore, H_{BIONIC} can be determined. However whether such a simple approach works or not highly depends on the simplicity of the native baroreflex system including the system linearity. We therefore examined the dynamic characteristics of baroreflex system.

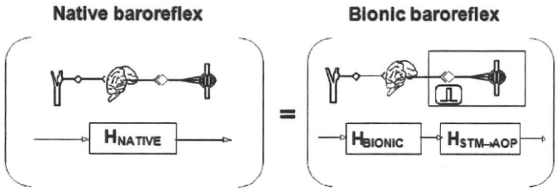

Fig. 1 Native vs. Bionic baroreflex

We vascularily isolated the baroreceptors (carotid sinuses) in rats (n=10) to open the baroreflex feedback loop and connected the carotid sinuses to a servo-controlled piston pump. This preparation allowed us to manipulate the carotid sinus pressure (CSP) independent of arterial pressure. We then perturbed CSP with random binary pressure sequences and identified the transfer function from CSP to arterial pressure. Shown in the left panels of Fig. 2 are the time series of CSP and aortic pressure. As can be seen, aortic pressure changes slowly toward the opposite direction in response to changes in CSP. This becomes even more evident in the transfer function (the right panel). The transfer function has low-pass filter characteristics. The phase response becomes nearly out-of-phase in the low frequency range suggesting the negative feedback nature of baroreflex system. Note that the magnitude squared coherence function is about 0.8 over the frequency range of interest. This is to say that most dominant characteristics of the total baroreflex open loop are captured by the linear transfer function.

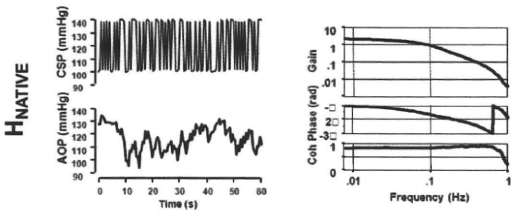

Fig. 2 Dynamic characteristics of native baroreflex system

In order to identify the actuator transfer function, we electrically stimulated the celiac ganglia with random binary pressure perturbations. Illustrated in the left panels of Fig. 3 are the time series of stimulation of celiac ganglia and aortic pressure responses. As can be seen, aortic pressure changes slowly toward the same direction in response to changes in stimulation. As anticipated the transfer function (the right panel) has low-pass filter characteristics. Unlike the total baroreflex loop, however, the phase response becomes nearly in-phase in the low frequency range. The magnitude squared coherence function is about 0.8 over the frequency range of interest. Again, it is reasonable to assume that most dominant characteristics of the actuator are captured by the linear transfer function.

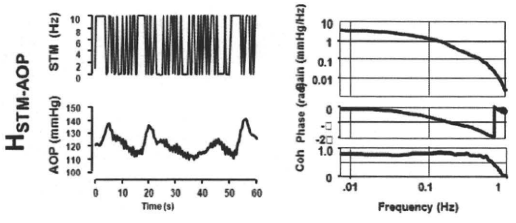

Fig. 3 Dynamic characteristics of sympathetic stimulation

We identified the transfer function (H_{BIONIC}) required for the controller by taking the ratio of H_{NATIVE} to $H_{STM \rightarrow AOP}$. Since both dynamic characteristics of the total baroreflex loop and actuator are well represented by the linear transfer functions, the resultant H_{BIONIC} should reproduce the native characteristics of the baroreflex system when the feedback loop is closed. Shown in Fig. 4 are the changes in arterial pressure in response to orthostatic stresses under the open-loop baroreflex condition (baroreflex failure), the closed-loop baroreflex condition (native baroreflex) and the bionic baroreflex condition. Orthostatic stresses profoundly lowered arterial pressure in the absence of the native baroreflex. Closing the native baroreflex loop markedly attenuated the hypotensive responses. The activation of bionic baroreflex system also attenuated the hypotensive response as much as the native baroreflex system did. Statistical analysis indicated that the pressure regulation achieved by the bionic baroreflex system was indistinguishable from that achieved by the native baroreflex system.

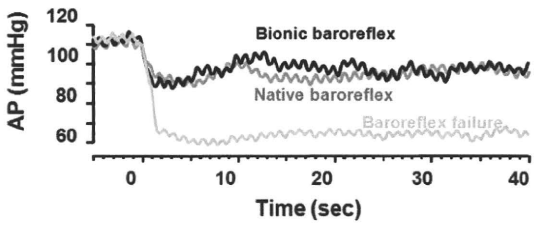

Fig. 4 Native baroreflex system vs. bionic baroreflex system

III. Discussion

We have shown that the bionic baroreflex system was as good as the native baroreflex system in regulating arterial pressure. The dynamic pressure responses to orthostatic stresses were indistinguishable between the native baroreflex system and the bionic baroreflex system. Although the baroreflex system is known to be nonlinear over the wide pressure range, we found that it is remarkably linear in the physiological pressure range. Because of this, the linear transfer function could represent the dominant characteristics of the baroreflex loop, and thereby allowed us to develop the bionic baroreflex system.

We can think of many anatomical sites where we can manipulate the activity of sympathetic system. In 1992, we stimulated the carotid sinus nerve to control the sympathetic system [1]. In 2004, we stimulated the spinal cord to stimulate the sympathetic efferent fibers [2]. The bionic mechanism worked beautifully regardless of the site of stimulation. It equally worked well in rats [3], rabbits [2], and dogs [1]. Although our experience of baroreflex failure in patients is limited, judging from its robustness, the bionic baroreflex system would work in patients as well [4]. If the bionic baroreflex system works in patients, it has a major impact as the treatment of baroreflex failure [5] that has been considered to be an incurable devastating disease.

IV. Conclusion

The bionic baroreflex system restores normal baroreflex function in an animal model of baroreflex failure.

ACKNOWLEDGMENT

This study was supported in part by Health and Labour Sciences Research Grant for Research on Medical Devices for Improving Impaired QOL from the Ministry of Health Labour and Welfare of Japan, Health and Labour Sciences Research Grant for Clinical Research from the Ministry of Health Labour and Welfare of Japan, and Grant-in-Aid for Scientific Research(S) (18100006) from the Japan Society for the Promotion of Science.

REFERENCES

[1] T. Kubota, H. Chishaki, T. Yoshida, K. Sunagawa, A. Takeshita, and Y. Nose, "How to encode arterial pressure into carotid sinus nerve to invoke natural baroreflex," *Am J Physiol* 263: H307-H313, 1992

[2] Y. Yanagiya, T. Sato, T. Kawada, M. Inagaki, T. Tatewaki, C. Zheng, A. Kamiya, H. Takaki, M. Sugimachi, and K. Sunagawa, "Bionic epidural stimulation restores arterial pressure regulation during orthostasis," *J Appl Physiol* 97: 984-990, 2004

[3] T. Sato, T. Kawada, T. Shishido, M. Sugimachi, and K. Sunagawa, "Novel therapeutic strategy against central baroreflex failure: A bionic baroreflex system," *Circulation* 100: 299-304, 1999

[4] F. Yamasaki, T. Ushida, T. Yokoyama, M. Ando, K. Yamasaki, and T. Sato, "Artificial baroreflex: clinical application of a bionic baroreflex system," *Circulation* 113: 634-639, 2008

[5] M. Sugimachi, and K. Sunagawa, "Bionic cardiology: exploration into a wealth of controllable body parts in the cardiovascular system," *IEEE Rev Biomed Eng.* 2: 172-186, 2009.

32nd Annual International Conference of the IEEE EMBS
Buenos Aires, Argentina, August 31 - September 4, 2010

Automated drug delivery system for the management of hemodynamics and cardiac energetic in acute heart failure

Kazunori Uemura, Masaru Sugimachi, *Member, IEEE*,
Toru Kawada, and Kenji Sunagawa, *Member, IEEE*

Abstract— **We have developed a novel automated drug delivery system for simultaneous control of systemic arterial pressure (AP), cardiac output (CO), and left atrial pressure (P_{LA}) in acute heart failure. The circulatory equilibrium framework we established previously discloses that AP, CO, and P_{LA} are determined by equilibrium of the mechanical properties of the circulation, i.e. pumping ability of the left heart, stressed blood volume and systemic arterial resistance. Our system directly controls the three mechanical properties with cardiovascular drugs including inotropes and vasodilators, thereby controlling AP, CO, and P_{LA}. Furthermore, by precisely controlling bradycardia and LV inotropy, our system enables to improve cardiac energetic efficiency while preserving AP, CO, and P_{LA} within acceptable ranges. In conclusion, by directly controlling the mechanical properties of the heart and vessel, our automated system realizes comprehensive management of hemodynamics in acute heart failure.**

I. Introduction

In the management of patients with acute heart failure after myocardial infarction or following cardiac surgery, cardiovascular agents such as inotropes and/or vasodilators are commonly used to control systemic arterial pressure (AP), cardiac output (CO) and left atrial pressure (P_{LA}). Since responses to these agents vary between patients and within patient over time, strict monitoring of patient condition and frequent adjustments of drug infusion rates are usually required. This is a difficult and time-consuming process, especially in hemodynamically unstable patients.

Although several closed-loop systems [1, 2] to automate drug infusion have been developed to facilitate this process, no closed-loop system so far developed is capable of controlling the overall hemodynamics; i.e., controlling AP, CO and P_{LA} simultaneously. This is because all previous systems attempted to directly control AP and CO by estimating response of the variable to drug infusion [1, 2]. This approach is inapplicable because of the difficulties to estimate simultaneous AP, CO and P_{LA} responses to the infusion of multiple drugs.

In this study, we developed a new automated drug delivery system to control AP, CO and P_{LA} [3]. To overcome the difficulty of the previous systems, our system adopted a strikingly original approach. We previously developed a circulatory equilibrium framework by extending the Guyton's classic framework [4]. As shown in Fig. 1, the extended framework consists of an integrated cardiac output curve characterizing the pumping ability of the left and the right heart, and a venous return surface characterizing the venous return property of the systemic and pulmonary circulation [5-7]. The intersection point of the integrated CO curve and the venous return surface predicts the equilibrium point of CO, P_{LA} and right atrial pressure (P_{RA}) (Fig. 1). Once CO, P_{LA} and P_{RA} are predicted from the intersection point, systemic arterial resistance determines AP. Based on this framework, instead of directly controlling AP, CO, and P_{LA}, our system controls the integrated CO curve with dobutamine (DOB), the venous return surface with 10% dextran 40 (DEX) and furosemide (FUR), and systemic arterial resistance with sodium nitroprusside (SNP), thereby controlling AP, CO and P_{LA}. The purpose of this study was, therefore, to develop and validate the automated drug delivery system.

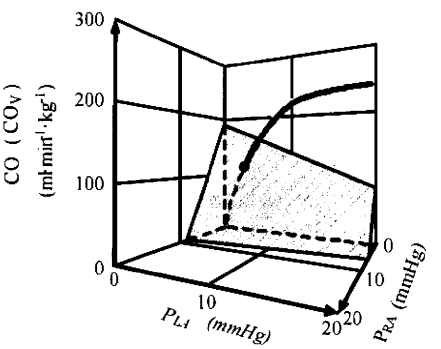

Fig. 1. Diagram of circulatory equilibrium for CO, venous return (CO_V), P_{LA}, and P_{RA}. The equilibrium CO, P_{LA} and P_{RA} are obtained as the intersection point of the venous return surface and integrated cardiac output curve.

Manuscript received April 23, 2010. This work was supported in part by Grant-in-Aid for Scientific Research (B 20300164, C 20500404) from the Ministry of Education, Culture, Sports, Science and Technology, by a research grant from Nakatani Foundation of Electronic Measuring Technology Advancement, by Health and Labour Sciences Research Grants (H20-katsudo-shitei-007) from the Ministry of Health Labour and Welfare of Japan.

K. Uemura, M. Sugimachi, and T. Kawada are with the National Cerebral and Cardiovascular Center Research Institute, Suita, Osaka 5658565, Japan.

K. Sunagawa is with Kyushu University, Fukuoka 8128582 Japan.

(corresponding author Kazunori Uemura, MD, PhD to provide phone: +81-6-6833-5012; fax: +81-6-6835-5403; e-mail: kuemura@ri.ncvc.go.jp).

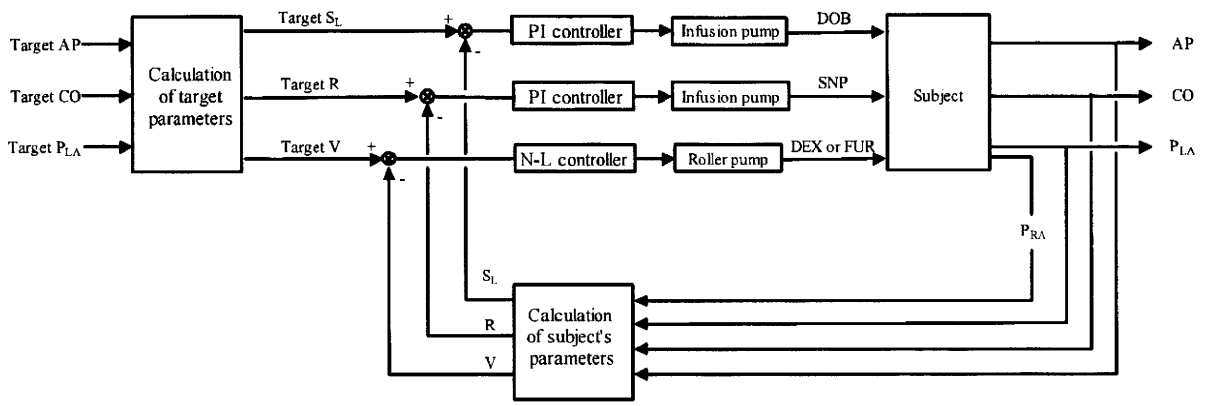

Fig. 2. Schematic illustration of an automated drug delivery system for simultaneous control of AP, CO and P_{LA}. Proportional-integral (PI) feedback controllers adjust infusion rate of DOB and SNP to minimize the difference between target and subject's S_L and those of R, respectively. Nonlinear (N-L) feedback controller adjusts infusion of DEX or injection of FUR to minimize the difference between target and subject's V.

In acute heart failure, cardiac energetic efficiency should also be improved. Theoretically, if heart rate (HR) is reduced while AP, CO and P_{LA} are maintained by preserving S_L with precisely increased LV contractility, it is possible to improve cardiac energetic efficiency and reduce LV oxygen consumption per minute (MVO_2) [8]. In the present study, we also investigated whether this hemodynamics can be accomplished in acute heart failure using our automated drug delivery system.

II. Methods

A. Automated drug delivery system

The integrated CO curve is parameterized by the pumping ability of the left heart (S_L) [ml·min^{-1}·kg^{-1}], the venous return surface by total stressed blood volume (V) [ml·kg^{-1}], and the systemic arterial resistance by R [mmHg·ml^{-1}·min·kg], which are calculated for a given set of AP, CO, P_{LA} and P_{RA} as the following formulas [3];

$$S_L = CO/[\ln(P_{LA} - 2.03) + 0.8] \quad (1)$$

$$V = (CO + 19.61P_{RA} + 3.49P_{LA}) \times 0.129 \quad (2)$$

$$R = (AP - P_{RA})/CO \quad (3)$$

Fig. 2 is a schematic illustration of the automated drug delivery system [3]. Once target values for AP, CO and P_{LA} are defined and fed into the computer, it calculates the target values for S_L, R, and V using Equations (1)-(3). The subject's S_L, R, and V are calculated from measured AP, CO and P_{LA} values using Equations (1)-(3). To minimize the differences between target and subject's S_L and R, proportional-integral feedback controllers adjust the infusion rates of DOB and SNP, respectively. To minimize the difference between target and subject's V, a nonlinear feedback controller adjusts the infusion of DEX or injection of FUR. Gain and rules of the controllers were predefined on the basis of the step responses of S_L, R, and V to the infusions of the drugs [3].

The adjustment processes are repeated in parallel and continued until the differences disappear.

B. Animal experiments to validate performance of the automated drug delivery system

In 12 anesthetized dogs, we acutely created ischemic heart failure by coronary embolization, which decreased CO from 133 ± 42 to 69 ± 22 ml·min^{-1}·kg^{-1}, AP from 109 ± 18 to 91 ± 17 mmHg and increased P_{LA} from 7 ± 2 to 19 ± 6 mmHg.

We connected the animals to the system, and defined target AP (90-105 mmHg), target CO (90-100 ml·min^{-1}·kg^{-1}) and target P_{LA} (8-12 mmHg), which were fed into the system to determine target values for S_L, R, and V as described above. The controllers were then activated by closing the loops. We observed the performance of the system over 50-60 min.

C. Circulatory equilibrium and cardiac energetics

S_L is theoretically related with LV end-systolic elastance (E_{es}, an index of LV contractility), HR, R and diastolic myocardial stiffness (k) as the following formula [7]

$$S_L = \frac{1}{k} \cdot \frac{E_{es}}{(E_{es}/HR) + R} \quad (4)$$

LV Stroke work (SW) is expressed as

$$SW = (AP - P_{LA}) \cdot CO/HR \quad (5)$$

LV pressure-volume area (PVA, an index of total mechanical energy of LV contraction) can be expressed as

$$PVA = AP \cdot AP/2E_{es} + SW \quad (6)$$

LV oxygen consumption per beat (BVO_2) is related to PVA and E_{es} as follows

$$BVO_2 = \alpha \cdot PVA + \beta \cdot E_{es} + \gamma \quad (7)$$

where α, β, and γ are constants. LV mechanical efficiency (ME) and oxygen consumption per minute (MVO_2) are expressed as follows:

$$ME = SW/BVO_2 \quad (8)$$

$$MVO_2 = BVO_2 \cdot HR \quad (9)$$

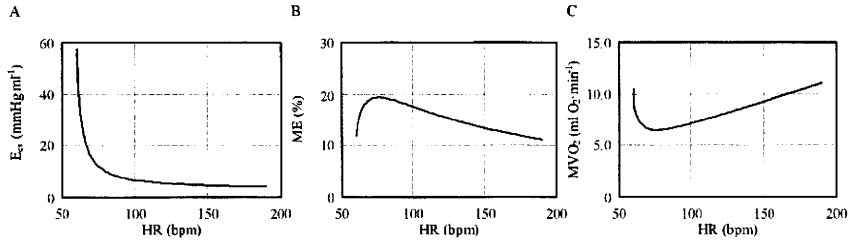

Fig. 3. Simulated relations of heart rate (HR) with left ventricular end-systolic elastance (E_{es}) (**A**), left ventricular mechanical efficiency (ME) (**B**), and left ventricular oxygen consumption per minute (MVO_2) (**C**), when AP, CO and P_{LA} are kept at fixed values.

Using Equations (4)-(9) and fixed values of AP (100 mmHg), CO (100 ml·min^{-1}·kg^{-1}) and P_{LA} (10 mmHg), we numerically simulated the individual relations of HR with E_{es}, ME and MVO_2 (Fig. 3). In these computations, representative k, α, β and γ values (not shown) were used, which are appropriate for a 20-kg dog.

As indicated in Fig. 3, HR is inversely related to E_{es} (Fig. 3A). Over the physiological range of HR for dogs (>80 bpm), ME increases as HR is reduced (Fig. 3B), i.e. cardiac energetic efficiency is optimized. At HR of 75 bpm, ME becomes maximal and MVO_2 becomes minimal (Fig. 3B, C). When HR is reduced from 150 to 110 bpm, E_{es} increases from 4.6 to 5.9 mmHg·ml^{-1} (29% increase) and ME increases from 13 % to 17 % (24 % increase), whereas MVO_2 decreases from 8.9 to 7.2 ml O_2·min^{-1} (19% reduction) [8]. This indicates that as long as HR is within the physiological range, HR reduction together with compensatory LV inotropy (an increase of E_{es}) consistently improves cardiac energetic efficiency and reduces MVO_2.

D. Animal experiments to optimize cardiac energetics using the automated drug delivery system

In 7 anesthetized dogs, we acutely created ischemic heart failure by coronary embolization, which decreased CO from 101±5 to 62±13 ml·min^{-1}·kg^{-1}, AP from 114±4 to 97±14 mmHg and increased P_{LA} from 9 ± 1 to 17±2 mmHg. Zatebradine (0.5 mg·kg^{-1}) was administered intravenously to suppress the intrinsic atrial beat, and atrial pacing was then initiated to control HR (146±8 bpm). After induction of acute heart failure, cardiac energetics were evaluated (*AHF*).

We activated the system with target values of 90-100 mmHg for AP, 80-100 ml/kg/min for CO and 10-12 mmHg for P_{LA}. The system restored AP, CO and P_{LA} to their respective target values within 30 min. After confirming stable hemodynamics, cardiac energetics were evaluated (*Initial HR*). We then reduced the pacing rate in steps of 10 or 20 bpm. The maximum HR reduction (*Lowest HR*) averaged 39±12 bpm. For each HR step, we waited for hemodynamic stabilization, and the measurements of cardiac energetics were performed.

III. Results

A. Performance of the automated drug delivery system

Fig. 4 shows the experimental trial in a representative animal. The system was activated at 0 min. Fig. 4A shows the time courses of the infusion rates of DOB and SNP, and the accumulated volume of infused DEX. In this case, FUR was not injected. Fig. 4B shows the time courses of S_L, R and V. Infusion rates of DOB, SNP, and DEX were adjusted so that S_L, R and V reached their respective target values. By controlling the cardiovascular parameters, the automated system controlled AP, CO and P_{LA} accurately and stably as demonstrated in Fig. 4C. AP, CO and P_{LA} reached their respective target levels within 30 min and remained at these levels.

In 12 animals, the average times for AP, CO and P_{LA} to reach the acceptable ranges (± 10 mmHg of target AP, ± 10 ml·min^{-1}·kg^{-1} of target CO, ± 2 mmHg of target P_{LA}) were 5.2 ± 6.6 min, 6.8 ± 4.6min, and 11.7 ± 9.8 min, respectively. The average standard deviations from the target values were small for AP [4.4 ± 2.6mmHg], CO [5.4 ± 2.4ml·min^{-1}·kg^{-1}] and P_{LA} [0.8 ± 0.6 mmHg].

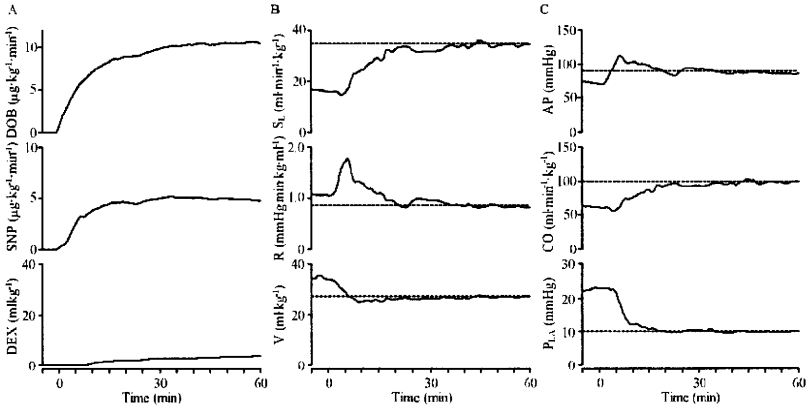

Fig. 4. Time courses of infusion rates of DOB and SNP, and cumulated volume of infused DEX (**A**), cardiovascular parameters (**B**), and hemodynamic variables (**C**) in one representative animal during closed-loop control of hemodynamics. Broken horizontal lines in panel B and C indicate target values.

B. Cardiac energetics improved following bradycardia while preserving normal hemodynamics in heart failure

In seven anesthetized dogs with acute heart failure, the automated drug delivery system restored and maintained normal hemodynamics (CO; 88±3 ml·min^{-1}·kg^{-1}, P_{LA};

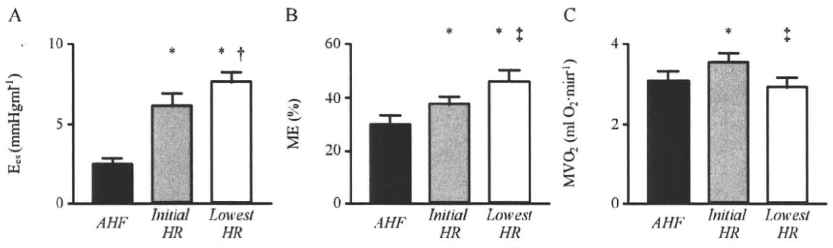

Fig. 5. Cardiac energetics after coronary artery embolization (*AHF*), at the initial HR (*Initial HR*), and at the lowest HR (*Lowest HR*). E_{es}, left ventricular (LV) end-systolic elastance; ME, LV mechanical efficiency; MVO_2, LV oxygen consumption per minute. Data are means ± SEM. *: $P<0.01$ vs *AHF*. †: $P<0.05$, ‡: $P<0.01$ versus *Initial HR*.

10.9±0.4 mmHg), even when zatebradine significantly reduced HR (107±7 bpm, -27±3%).

Fig. 5 summarizes cardiac energetics at *AHF*, *Initial HR*, and *Lowest HR*. When the data at *Initial HR* and *Lowest HR* were compared with those at *AHF*, E_{es} and ME increased significantly. MVO_2 at *Initial HR* also increased compared to that at *AHF*, although MVO_2 at *Lowest HR* was almost identical to that at *AHF*. The automated drug delivery system restored normal hemodynamics with increased energy cost at *Initial HR*, but with diminished energy cost at *Lowest HR*. Comparing the data at *Lowest HR* with those at *Initial HR*, E_{es} increased (+34±14 %), ME increased (+22±6 %) and MVO_2 decreased significantly (-17±4 %). Changes in the LV mechanoenergetic data following HR reduction averaged over seven animals are compatible with those predicted theoretically (Fig. 3).

IV. Discussion

A. Characteristics of our system

Our system controls the mechanical determinants of circulation, and as a result achieves target values for hemodynamic variables [3]. Previous systems attempted to control hemodynamic variables by estimating the apparent input–output relations between drug infusion and response of the controlled variables. In the systems that control AP and CO, all possible input–output relations have to be estimated; namely, inotrope–AP, inotrope–CO, vasodilator–AP, and vasodilator–CO relations [2]. The reason is that these drugs affect AP and CO simultaneously to almost the same degree. If this previous approach is applied to simultaneous control of AP, CO and P_{LA}, at least 9 input–output relations have to be estimated, since at least 3 drugs are required to independently control the three variables. This would make the system extremely complicated, and therefore be practically unfeasible. The three drug controllers in our system (Fig. 2) are designed on the basis of only three input–output relations between drug infusion and response of the controlled parameter; namely, DOB–S_L, SNP–R and DEX/FUR–V. The fact that the three closed loops are effectively decoupled simplifies the entire system. This also permits a system operator, who would be a physician untrained in control engineering, to understand its behavior easily

B. Simultaneous optimization of cardiac energetic and hemodynamics

The degree of reduction in MVO_2 (17 %, *Lowest HR* vs *Initial HR* in Fig. 5C) when HR was reduced by 30% in the present experiment is less than that observed in beta-blockade treatment. For example, atenolol decreased MVO_2 by 40% when HR was reduced by 30% in dogs during exercise. Negative ventricular inotropy accompanying HR reduction accounts for the further reduction in MVO_2 achieved by beta-blockade. However, in acute heart failure, use of beta-blockers is contraindicated owing to its adverse effects on systemic hemodynamics. Taken together, the degree of reduction in MVO_2 obtained in this study is reasonable considering that it is achieved without sacrificing the normal hemodynamic condition.

V. Conclusion

By directly controlling the mechanical properties of the heart and vessel, our automated system enables comprehensive management of hemodynamics in acute heart failure.

References

[1] W. R. Chitwood Jr., D. M. Cosgrove 3rd., R. M. Lust, "Multicenter trial of automated nitroprusside infusion for postoperative hypertension. Titrator Multicenter Study Group," *Ann. Thorac. Surg.* vol. 54, no. 3, 517-522, Sep. 1992.

[2] C. Yu, R. J. Roy, H. Kaufman, B. W. Bequette, "Multiple-model a daptive predictive control of mean arterial pressure and cardiac output," *IEEE. Trans. Biomed. Eng.* vol. 39:765-778, 1992.

[3] K. Uemura, A. Kamiya, I. Hidaka, T. Kawada, S. Shimizu, *et al.*, "Automated drug delivery system to control systemic arterial pressure, cardiac output, and left heart filling pressure in acute decompensated heart failure," *J. Appl. Physiol.* vol. 100, no 4, 1278-1286, Apr. 2006.

[4] A. C. Guyton, "Determination of cardiac output by equating venous return curves with cardiac response curves," *Physiol. Rev.* vol. 35, no. 1,123–129, Jan. 1955.

[5] K. Sunagawa, K. Sagawa, W. L. Maughan, "Ventricular interaction with the loading system," *Ann. Biomed. Eng.* vol. 12, no. 2, 163-189, 1984.

[6] K. Uemura, M. Sugimachi, T. Kawada, A. Kamiya, Y. Jin, *et al.*, "A novel framework of circulatory equilibrium," *Am. J. Physiol. Heart Circ. Physiol.* vol. 286, no. 6, pp. H2376–H2385, Jun. 2004.

[7] K. Uemura, T. Kawada, A. Kamiya, T. Aiba, I. Hidaka, *et al.*, "Prediction of circulatory equilibrium in response to changes in stressed blood volume," *Am. J. Physiol. Heart Circ. Physiol.* vol. 289, no. 1, H301–H307, Jul. 2005.

[8] K. Uemura, K. Sunagawa, M. Sugimachi, "Computationally managed bradycardia improved cardiac energetics while restoring normal hemodynamics in heart failure," *Ann. Biomed. Eng.* vol. 37, no. 1, 82-93, Jan. 2009.

Early Short-Term Vagal Nerve Stimulation Attenuates Cardiac Remodeling After Reperfused Myocardial Infarction

KAZUNORI UEMURA, MD, PhD,[1] CAN ZHENG, PhD,[2] MEIHUA LI, PhD,[1]
TORU KAWADA, MD, PhD,[1] AND MASARU SUGIMACHI, MD, PhD[1]

Suita, Japan; Nankoku, Japan

ABSTRACT

Background: Vagal nerve stimulation (VS) has been suggested to be an effective adjunct to reperfusion therapy in myocardial infarction (MI). However, the effect of VS on left ventricular (LV) remodeling after reperfused MI has not been examined.

Methods and Results: We investigated the effects of early, brief VS on acute inflammatory reactions (study 1) and chronic LV remodeling (study 2) in a rabbit model of reperfused MI. In study 1, rabbits were subjected to 60-minute coronary artery occlusion followed by reperfusion alone (MI, n = 8) or treated with 24-hour VS (MI-VS, n = 8). At 24 hours after ischemia-reperfusion, MI-VS rabbits showed significantly decreased myocardial infiltration of neutrophils and reduced myocardial expressions of tumor necrosis factor-α and matrix metalloproteinase-8 and -9, compared with MI rabbits. Myocardial expression of interleukin-6 was not affected by VS. In study 2, rabbits were subjected to coronary occlusion and reperfusion alone (n = 16) or treated with VS for 3 days (n = 14). At 8 weeks after ischemia-reperfusion, MI-VS rabbits showed significantly improved LV dysfunction and dilatation, and significantly reduced infarct size, infarct wall thinning, and LV weight compared with MI rabbits.

Conclusion: Early, short-term VS attenuates LV remodeling after reperfused MI, which may be associated with suppression of acute inflammatory reactions. (*J Cardiac Fail 2010;16:689–699*)

Key Words: Hypertrophy, cardiac function, acute inflammatory response, matrix metalloproteinase.

Left ventricular (LV) myocardial remodeling that occurs after myocardial infarction (MI) leads to progressive LV dilation and eventually pump dysfunction, and is one of the major determinants of long-term survival after MI.[1] In patients with acute MI, reperfusion of the ischemic tissue is the primary therapeutic strategy, and reduction of infarct size afforded by reperfusion contributes to improved clinical outcomes.[2] However, a substantial population of patients with MI still develops LV remodeling and heart failure even after reperfusion therapy.[1,2] Therefore some novel therapeutic modality should be developed as an adjunct to reperfusion therapy to attenuate chronic LV remodeling and improve the long-term outcome of MI patients.

A previous communication from our laboratory reported that electrical stimulation of vagal nerve (VS) for 6 weeks ameliorated LV remodeling and improved survival in a rat model of non-reperfused MI.[3] A small pilot clinical study demonstrated the beneficial effect of long-term, 6-month VS on LV function in patients with heart failure.[4] Several acute phase experimental studies also indicated the cardioprotective effects of VS in myocardial ischemia-reperfusion injury.[5–7] All these results strongly suggest that VS may be an effective adjunct to reperfusion therapy in patients with MI. However, the antiremodeling effect of VS remains poorly characterized and the effect on reperfused MI has not been examined.

Inflammatory cytokines are important mediators of LV remodeling after MI. Tumor necrosis factor-α (TNF-α) is an essential cytokine that is produced in significant quantities within the infarcted myocardium very soon after MI, and contributes to LV remodeling by inducing intense local inflammatory response, matrix metalloproteinase (MMP) activities, and matrix degradation.[8,9] VS has been shown

From the [1]Department of Cardiovascular Dynamics, Advanced Medical Engineering Center, National Cardiovascular Center Research Institute, Suita, Japan and [2]Department of Cardiovascular Control, Kochi Medical School, Nankoku, Japan.

Manuscript received October 9, 2009; revised manuscript received February 19, 2010; revised manuscript accepted March 2, 2010.

Reprint requests: Kazunori Uemura, MD, PhD, Department of Cardiovascular Dynamics, Advanced Medical Engineering Center, National Cardiovascular Center Research Institute, 5-7-1 Fujishirodai, Suita 565-8565, Japan. Tel: +81-6-6833-5012 (ext. 2414); Fax: +81-6-6835-5403. E-mail: kuemura@ri.ncvc.go.jp

See page 698 for disclosure information.

1071-9164/$ - see front matter

doi:10.1016/j.cardfail.2010.03.001

to attenuate hepatic and cardiac TNF-α synthesis in splanchnic artery reperfusion injury or lethal endotoxemia.[10,11] We[12] and LaCroix et al[13] have demonstrated that VS induces expression of tissue inhibitor of MMP (TIMP)-1 and reduces active MMP-9 in ischemic myocardium. Although these findings suggest that VS favorably modulates the inflammatory reactions in MI, the effects of VS on inflammatory responses including the expression of cytokines and MMPs as well as its association with the inflammatory cell infiltrations have not been investigated in the setting of MI.

Long-term VS requires permanent implantation of the entire stimulating system.[3,4] However, hemodynamically unstable patients with acute MI are poor surgical candidates. On the other hand, early brief VS via an intravascular[14] or a transcutaneous approach[11] without compromising the hemodynamic conditions would be feasible in acute clinical settings. Taking all these together, the objective of this study was to investigate the effects of early short-term VS on LV function and myocardial structural remodeling in a rabbit model of reperfused MI and their association with acute inflammatory reactions.

Methods

Animals

We used a total of 56 Japanese white rabbits in this study (male, 2.5 to 3.0 kg). The investigation conforms with the *Guide for the Care and Use of Laboratory Animals* published by the US National Institutes of Health (NIH Publication No. 85-23, revised 1996). All protocols were approved by the Animal Subjects Committee of the National Cardiovascular Center (approval number: 8042). Rabbits were assigned to the MI group (left coronary artery occlusion and reperfusion only; n = 24), MI-VS group (left coronary artery occlusion and reperfusion plus early short-term VS; n = 22), and normal control (NC) group (no treatment; n = 10).

Implantation of Vagal Nerve Electrode

Rabbits in the MI-VS group were implanted with vagal nerve electrodes. Under general anesthesia (sodium pentobarbital, 35 mg/kg $^{-1}$) and mechanical ventilation, a pair of polyurethane-coated stainless steel wires for electrical stimulation was looped around the right vagal nerve in the neck region.[3] The electrode wires were tunneled beneath the skin, exited in the midscapular area, and connected to a radio-controlled pulse generator (SRG-3100, Nihon Kohden, Japan) placed in a nylon jacket. Rabbits in the MI group underwent sham surgery without implanting the electrode. The animals were allowed to recover for at least 1 week before induction of MI (Fig. 1).

Induction of MI

MI was induced in rabbits of the MI and MI-VS groups (Fig. 1). Under general anesthesia (sodium pentobarbital, 35 mg/kg^{-1}) and mechanical ventilation with room air, a left thoracotomy was performed. A 4-0 proline suture was passed around the circumflex coronary artery, and a snare was formed by passing the ends of the thread through a small vinyl tube.[12] Electrodes to record surface electrocardiogram were implanted subcutaneously. The circumflex tourniquet was tightened to completely stop blood flow as demonstrated by both electrocardiogram changes and visual blanching of the myocardium. In the MI-VS group, we started vagal nerve stimulation immediately after coronary occlusion using rectangular pulses of 1-ms duration at 20 Hz for 10 seconds every minute.[3] We adjusted the amplitude of the pulse in each animal to reduce heart rate (HR) by 10% from baseline value. Consequently, the amplitudes ranged from 2 to 8 V. In a preliminary study, we confirmed that VS at this intensity did not alter feeding behavior and did not evoke any sign of pain reaction. After 60 minutes of coronary occlusion, the tourniquet was released, allowing reperfusion in both groups. The chest wall was then closed, and the animal was allowed to recover.

After recovery from anesthesia of MI surgery, we checked HR response to VS in MI-VS rabbits by monitoring electrocardiogram at least twice per day under conscious condition. We readjusted the intensity of VS if necessary, because the response varied from day to day in an individual rabbit.

Experimental Protocols

We performed 2 studies (Fig. 1). In study 1, VS was continued for 24 hours in MI-VS rabbits, and the effects of VS on myocardial inflammatory reactions at 24 hours after coronary reperfusion were examined because myocardial expression of TNF and MMP-9 as well as infiltration of neutrophil have been shown to peak at around 24 hours after myocardial ischemia reperfusion.[15] In study 2, VS was continued for 3 days in MI-VS rabbits, and LV function and structure were examined at 8 weeks after coronary reperfusion.

Study 1: Acute Phase after MI

Study 1 consisted of 3 groups of rabbits: MI (n = 8), MI-VS (n = 8), and NC (n = 3). At 24 hours after coronary reperfusion, animals in the MI and MI-VS groups were euthanized and whole hearts were harvested.

Western Blot. Myocardial tissue sample obtained from the LV lateral wall (infarct region in MI and MI-VS rabbits) was homogenized in RIPA lysis buffer (Rockland, Gilbertsville, PA) containing proteinase inhibitor (Complete Mini, Roche, Basel, Switzerland). The homogenate was centrifuged at 4 °C at 2000g for 10 minutes and the resultant supernatant was further subjected to centrifugation at 12,000g for 20 minutes. Protein concentration of each supernatant sample was determined using a DC Protein assay kit (BioRad Hercules, CA).

Samples containing equal amounts of protein (25 μg) were separated on 15% sodium dodecyl sulfate polyacrylamide gel electrophoresis gel (Bio-Rad) and transferred onto Immobilon-P membrane (Millipore, Billerica, MA). After blocking the membranes with BlockAce (Dainippon Pharmaceutical, Japan), TNF-α was detected with polyclonal antibody for TNF-α (sc-1348, Santa Cruz, CA) and donkey-anti-goat HRP (sc-2020, Santa Cruz). Interleukin-1β (IL-1β) was detected with polyclonal antibody for IL-1β (LS-C7719, LifeSpan Biosciences, Seattle, WA) and goat-anti-rabbit HRP (sc-2004, Santa Cruz). MMP-1, MMP-7, MMP-8, and β-actin were detected using monoclonal antibodies for MMP-1 (F-67, Daiichi Fine Chemical, Japan), MMP-7 (F82, Daiichi Fine Chemical), MMP-8 (F-83, Daiichi Fine Chemical), and β-actin (sc-47778, Santa Cruz), respectively, and goat-anti-mouse HRP (sc-2005, Santa Cruz). Protein bands were visualized with ECL Plus (GE Healthcare, UK), and analyzed using a densitometric analysis software (CS Analyzer 3.0, ATTO, Japan). Band densities were standardized to β-actin, and presented as percent

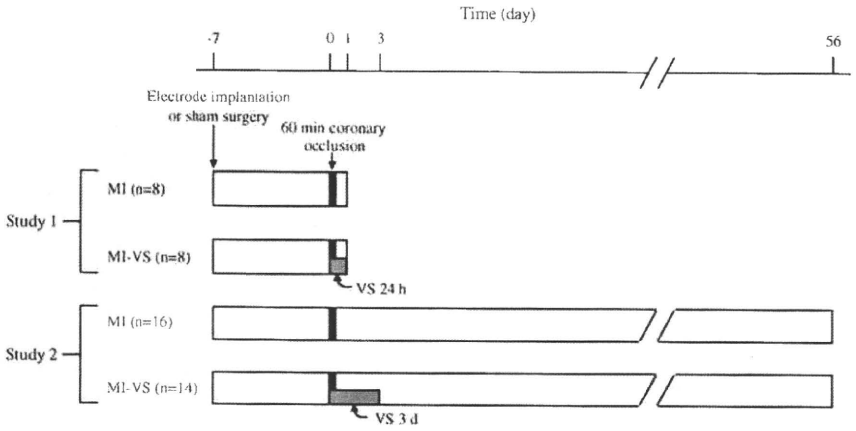

Fig. 1. Schematic representation of the protocols of Study 1 (acute phase myocardial infarction and reperfusion) and Study 2 (chronic phase after creation of reperfused myocardial infarction). MI, rabbits with reperfused myocardial infarction; MI-VS, MI rabbits treated with vagal nerve stimulation. Three rabbits in Study 1 and 7 rabbits in Study 2 were used as normal controls (not shown in this figure).

change compared with NC values, the means of which were arbitrarily set as 100%.

Enzyme-Linked Immunosorbent Assay. Myocardial tissue sample obtained from the LV lateral wall (infarct and peri-infarct regions in MI and MI-VS rabbits) was homogenized and processed as described previously.

Enzyme-linked immunosorbent assays for C-reactive protein (CRP) (KT-097, Kamiya Biomedical Company, Seattle, WA) and TIMP-1 (RPNJ409, Daiichi fine chemical) were performed using the supernatants of myocardial tissue homogenates from the infarct region according to the manufactures' instructions.[12] Enzyme-linked immunosorbent assays for IL-6 (900-033, Assay Designs, Ann Arbor, MI) was performed using the supernatants of myocardial tissue homogenates from the peri-infarct region. The reason for using the peri-infarct region instead of the infarct region for IL-6 measurement was based on a previous finding that IL-6 mRNA is intensely induced in myocytes of the viable border zone, and not the necrotic infarct zone in myocardial ischemia-reperfusion.[16]

Gelatin Zymography. Tissue sample from the LV lateral wall was homogenized in lysis buffer (50 mM Tris, pH 7.4). The homogenate was centrifuged at 2000*g* for 10 minutes at 4 °C and the supernatant was collected. Protein concentration of each supernatant sample was determined as described previously.

Gelatin zymography was performed to assess the relative contents of the gelatinases MMP-2 and MMP-9 as described previously.[12] The supernatants (30 μg protein) were loaded in Novex gels containing 0.1% gelatin (Invitrogen, Carlsbad, CA) and then electrophoresed. After renaturation, equilibration, and incubation for 20 hours at 37 °C in developing buffer, the gels were stained in 0.5% Coomassie Blue G-250. Gels were dried and scanned. MMP-2– and MMP-9–related bands were analyzed using the densitometric analysis software.

Determination of Neutrophil Infiltration. The middle ring slice of LV was embedded in paraffin, sectioned at a thickness of 5 μm, and stained with hematoxylin and eosin. We counted the numbers of neutrophils per field in the infarcted area. Neutrophil infiltration into ischemic myocardium was also quantified by evaluating myeloperoxidase activity. Tissue sample from the LV lateral wall was homogenized in potassium phosphate buffer (50 mM, pH 6.4) containing 0.5% hexadecyltrimethylammonium bromide (WAKO, Japan). The homogenate was centrifuged at 4 °C at 12,000*g* for 10 minutes and the resultant supernatant was reacted with 0.167 mg/mL of o-dianisidine dihydrochloride (Sigma-Aldrich, St. Louis, MO) and 0.0005% H_2O_2 in potassium phosphate buffer. The change in absorbance at 450 nm was measured spectrophotometrically over 2 minutes. One unit of myeloperoxidase activity was defined as that quantity of enzyme that hydrolyzed 1 μM of peroxide per minute at 25 °C.

Study 2: Chronic Phase after MI

Study 2 consisted of 3 groups of rabbits: MI (n = 16), MI-VS (n = 14), and NC (n = 7).

Echocardiography. Echocardiography was performed under conscious condition at baseline and at 3 days and 8 weeks after coronary reperfusion. Two-dimensional, targeted M-mode tracings were obtained at the level of the papillary muscles with an echocardiographic system equipped with a 7-MHz transducer (Power Vision, TOSHIBA, Japan). LV dimensions were measured according to the American Society for Echocardiography leading-edge method for at least 3 consecutive cardiac cycles. Fractional shortening was calculated as (LVEDD-LVESD)/LVEDD×100, where LVEDD is LV end-diastolic diameter and LVESD is LV end-systolic diameter.

Hemodynamic and Plasma MMPs Measurements. Hemodynamic measurements were performed at 8 weeks after reperfusion. Under general anesthesia (sodium pentobarbital, 35 mg/kg^{-1}) and mechanical ventilation with room air, a 3F micromanometer-tipped catheter (Millar Instruments, Houston, TX) was inserted into the right carotid artery for measurement of mean arterial pressure. Next, the catheter was advanced into the LV for measurement of LV pressure. After completing these measurements, blood was sampled from the right carotid artery. The animal was euthanized. The whole heart was quickly excised and washed with cold phosphate-buffered saline.

Relative protein contents of MMP-2 and MMP-9 in plasma were measured with use of the gelatin zymography as described previously.

LV Passive Pressure-volume Relationship. The excised heart was perfused with a cold, hypocalcemic, hyperkalemic cardioplegic solution (NaCl: 130 mM, KCl: 20 mM, $CaCl_2$: 0.08

mM, lidocaine: 0.5 μg/mL; pH 7.3; 310 mOsm). The passive LV pressure-volume relationship of the arrested heart was measured as described previously.[17] In brief, a compliant water-filled latex balloon tied on a rigid Y-connector was placed in the left ventricle and secured at the mitral annulus with a purse-string suture. Pressure within each balloon was measured with a catheter-tipped micromanometer (Millar Instruments) as volume was progressively increased. Pressure was then plotted as a function of volume at each step, resulting in a passive pressure-volume relationship equivalent to the end-diastolic pressure-volume relationship of the beating heart.[17] The size of the left ventricle was indexed by the volume at which LV pressure reached 10 mm Hg (LVV_{10}).

Infarct Characterization. The coronary branch was reoccluded and 5 mL 0.25% Evans blue was injected from the aorta at 80 mm Hg. After the vasculature, right ventricular free wall, and atrial appendages were dissected, the left ventricle was weighed and fixed in 4% paraformaldehyde overnight. The left ventricle below the coronary artery ligation site was cut into ~5 transverse slices parallel to the atrioventricular ring. Each slice was photographed. The risk area unstained by the blue dye and the non-risk area stained by the blue dye were demarcated. For each slice, the risk area size was determined as the total circumference of the risk area divided by total LV circumference (in percent). The risk area sizes of all slices were averaged and expressed as the risk area size for each heart. The fixed slices from the apex, middle ring, and base were then embedded in paraffin and sectioned at a thickness of 5 μm.

The 5-μm thick cross-sections of left ventricle were stained with Masson's trichrome and Sirius red. Using sections stained with Masson's trichrome, infarct size was determined as the total infarct circumference divided by total LV circumference (in percent). The thicknesses of septal (non-infarct area) and LV lateral walls (infarct area) were measured. The thinning ratio, an index of the extent of wall thinning in the infract, is calculated by dividing the infarct wall thickness by septal wall thickness. Cardiomyocyte cross-sectional areas were determined in the non-infarcted septal myocardium. Only cardiomyocytes cut in cross section were measured. Using sections stained with Sirius red, collagen densities in noninfarcted regions were determined as described previously.[18] Histological images were obtained with a microscope system (BZ 9000, Keyence, Japan), and analyzed using the National Institutes of Health Image software (Image J 1.37). The infarct sizes of the 3 sections (apex, middle ring, base) were averaged and expressed as the LV infarct size for each heart. The thickness of LV wall, cardiomyocyte cross-sectional area, and collagen density were determined in the section that most clearly transverses the infarct region.

Statistical Analyses

All data are presented as mean ± SEM values. Mortalities in the MI and MI-VS groups were compared using chi-square test. Between-group comparison of means obtained at a single time point was performed by Student's unpaired *t*-test or 1-way analysis of variance. Between-group comparisons of the changes of means over time were conducted using two-way repeated measure analysis of variance to examine any group-time effect. All analyses of variance showing significant differences were further analyzed by post hoc comparison using Student-Newman-Keuls test (Statistica, Statsoft, Inc., Tulsa, OK). *P* values less than .05 were considered statistically significant.

Results

Study 1: Acute Phase after MI

Body Weight and Mortality. Baseline body weight were comparable among the NC (2490 ± 38 g), MI (2656 ± 64 g), and MI-VS (2517 ± 31 g) groups. Two MI and 2 MI-VS rabbits died from arrhythmia at MI induction. There was no difference in mortality rate up to 24 hours after coronary reperfusion between the MI and MI-VS groups (25% vs. 25 %, P = NS).

HR. Changes of HR over time are summarized in Table 1. There were no significant differences in HR between the MI and MI-VS groups at baseline, after 30 minutes of coronary occlusion, and at 24 hours after coronary reperfusion. No significant time effects on HR were observed.

Myocardial Expression of Cytokines, MMPs, and CRP. Figure 2A shows representative Western blots for TNF-α in the infarcted myocardium. Densitometric analysis demonstrated that TNF-α protein level increased significantly in the MI and MI-VS groups compared with NC value, whereas TNF-α level in the MI-VS group was significantly lower than that in the MI group (<50%, $P < .05$, Fig. 2A). Myocardial protein expressions of IL-1β and IL-6 are summarized in Table 2. There were no significant differences in IL-1β level among the 3 groups. Myocardial levels of IL-6 increased significantly to similar degrees in the MI and MI-VS groups compared with NC values.

As shown in Fig. 2B, zymography of the myocardial extracts detected 2 bands at 92 kDa and 72 kDa corresponding to pro-MMP-9 and pro-MMP-2, respectively. In 2 of 11 MI hearts, but in none of 10 MI-VS hearts, a faint gelatinolytic band was also observed at 83 kDa, which presumably represents the active form of MMP-9.[19] To evaluate the relative content of MMP-9, we used the 92 kDa band (pro-MMP-9) because this band is representative of the global MMP-9 activity.[20] Relative MMP-9 level increased significantly in the MI and MI-VS groups compared with NC value. Level of MMP-9 in the MI-VS group was significantly lower than that in the MI group (<40%, $P < .05$, Fig. 2B). There were no significant differences in MMP-2 (pro-MMP-2) protein level among the 3 groups. Western

Table 1. Changes of Heart Rate with Time after Myocardial Ischemia-reperfusion (Studies 1 and 2)

	Baseline	30 Minutes	24 Hours	3 Days
Study 1				
MI	(n = 6)	277 ± 8	244 ± 24	257 ± 12
MI-VS	(n = 6)	256 ± 8	243 ± 6	250 ± 7
Study 2				
MI	(n = 11)	268 ± 10	245 ± 10	309 ± 11*†
MI-VS	(n = 10)	264 ± 22	224 ± 11	313 ± 15†

MI, myocardial infarction; MI-VS, myocardial infarction treated with vagal nerve stimulation; 30 minutes, 30 minutes after coronary occlusion; 24 hours, 24 hours after coronary reperfusion; 3 days, 3 days after coronary reperfusion.

Heart rate data (beat/min) are means ± SEM.

*$P < .05$ versus baseline.

†$P < .01$ versus 30 minutes.

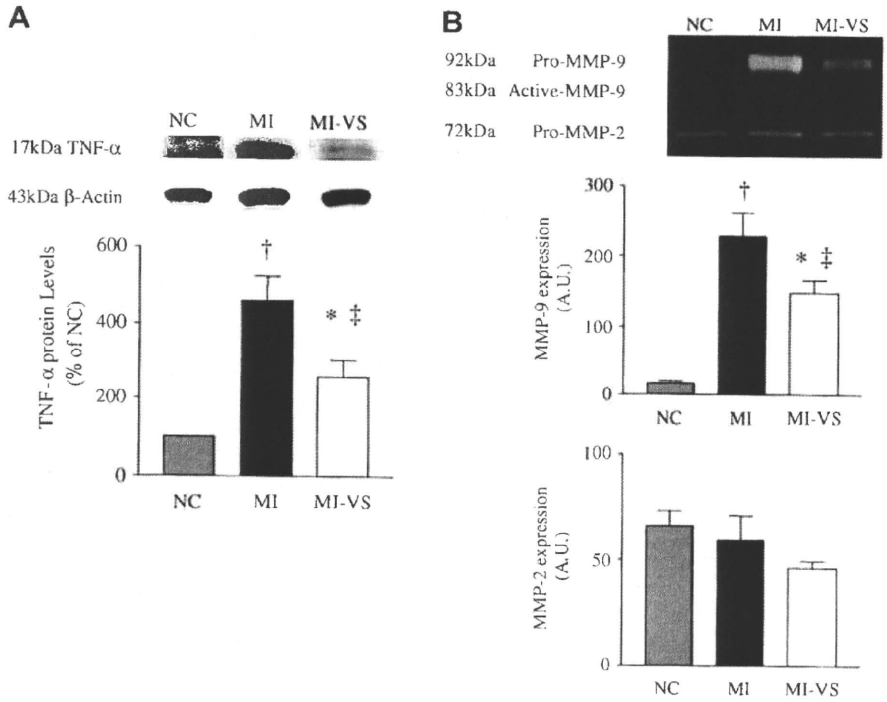

Fig. 2. Myocardial protein expressions of tumor necrosis factor-α (TNF-α) and matrix metalloproteinases (MMPs) in normal control rabbits (NC, n = 3), rabbits with reperfused myocardial infarction (MI) (n = 6), and MI rabbits treated with vagal nerve stimulation (MI-VS) rabbits (n = 6). (A) Representative Western blots of TNF-α (17 kDa) as well as corresponding β-actin bands (43 kDa) and band intensities normalized to NC values are shown. (B) Representative zymogram shows pro-MMP-9 band at 92 kDa and pro-MMP-2 band at 72 kDa. Note the faint 83 kDa band in MI hearts, which represents active MMP-9. Densitometric analysis of MMP-9 and MMP-2 contents expressed in integrated optical density (A.U.) relative to background. Data are means ± SEM. $^{*}P < .05$, $^{\dagger}P < .01$ versus NC. $^{\ddagger}P < .05$ versus MI.

blot analysis of other species of MMPs is summarized in Table 2. Myocardial protein levels of MMP-1 (50 kDa, pro-MMP-1) and MMP-7 (28 kDa, pro-MMP-7) decreased significantly to similar degrees in the MI and MI-VS groups compared to NC values. Myocardial protein level of MMP-8 (75 kDa, pro-MMP-8) increased significantly in the MI group compared with NC and MI-VS values (Table 2).

Table 2. Myocardial Protein Expression (Study 1)

	NC (n)	MI (n)	MI-VS (n)
IL-1β, % of NC	100 ± 6 (3)	79 ± 8 (6)	105 ± 25 (5)
IL-6, ng/g protein	52 ± 2 (3)	100 ± 7 (3) *	97 ± 13 (4)*
MMP-1, % of NC	100 ± 6 (3)	54 ± 8 (6) †	71 ± 12 (6)*
MMP-7, % of NC	100 ± 18 (3)	40 ± 10 (3) *	18 ± 2 (3)‡
MMP-8, % of NC	100 ± 15 (3)	510 ± 82 (3) †	236 ± 65 (3)‡
TIMP-1, ng/g protein	39 ± 1 (3)	1394 ± 101 (6)†	1387 ± 164 (6)†
CRP, μg/g protein	13 ± 3 (3)	1926 ± 225 (6)†	1741 ± 114 (6)†

IL, interleukin; MMP, matrix metalloproteinase; TIMP, tissue inhibitor of metalloproteinase; CRP, C-reactive protein.

Data are means ± SEM. The number of hearts used for each experiment is given in parentheses.

$^{*}P < .05$.

$^{\dagger}P < .01$ versus NC.

$^{\ddagger}P < .05$ versus MI.

Myocardial level of TIMP-1 protein increased significantly to similar degrees in MI and MI-VS groups compared with NC values (Table 2).

Myocardial level of CRP increased significantly to similar degrees in the MI and MI-VS groups compared with NC values (Table 2).

Neutrophil Infiltration. No myocardial neutrophil infiltration was found in NC rabbits, whereas intense neutrophil infiltration into the infarcted myocardium was observed in MI rabbits (Fig. 3A). On the other hand, a significantly reduced neutrophil density in the infarcted myocardium was evident in MI-VS rabbits compared with MI animals (Fig. 3A, B). In accordance with neutrophil counts, myeloperoxidase activity in MI-VS rabbits was significantly reduced compared with MI animals (Fig. 3C).

Study 2: Chronic Phase after MI

Body Weight and Survival. Baseline body weights were comparable among the NC (2693 ± 184 g), MI (2530 ± 38 g), and MI-VS (2462 ± 24 g) groups. At 3 days after coronary reperfusion, body weights decreased to the same extent in both the MI (2325 ± 38 g) and MI-VS (2361 ± 53 g) groups. At 8 weeks after reperfusion, body weights increased to similar degrees in the MI (2843 ± 69 g) and

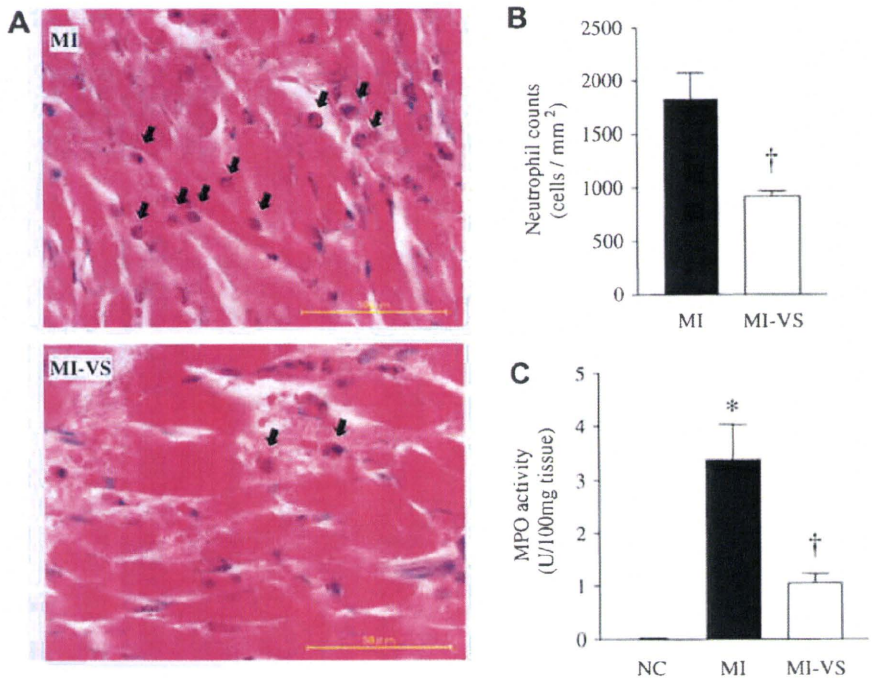

Fig. 3. (A) Photomicrographs of hematoxylin-eosin stained left ventricle cross-sections in infarcted regions obtained from rabbits with reperfused myocardial infarction (MI) and MI rabbits treated with vagal nerve stimulation (MI-VS) rabbits at 24 hours after coronary reperfusion. Arrows indicate infiltrating neutrophils. Bars = 50 μm. (B) Neutrophil counts of sections in infarct regions from MI (n = 6) and MI-VS (n = 6) rabbits. (C) Myocardial myeloperoxidase (MPO) activity in NC rabbits (n = 3), and in the infarct regions from MI (n = 4) and MI-VS (n = 4) rabbits. $^{*}P < .01$ versus NC, $^{\dagger}P < 0.01$ versus MI.

MI-VS (2899 ± 53 g) groups compared with the respective baseline values.

Five MI and four MI-VS rabbits died and the mortality rate up to 8 weeks after coronary reperfusion was comparable between the MI and MI-VS groups (31% versus 29%, P = NS). Of these deaths, 2 MI (13%) and 3 MI-VS (21%) rabbits died from arrhythmia at MI induction (P = NS).

Hemodynamics and LV Function. HR at 3 days after coronary reperfusion significantly increased in both the MI and MI-VS groups from their respective baseline values (Table 1). There were no significant differences in HR between the MI and MI-VS groups at baseline, after 30 minutes of coronary occlusion, and at 3 days after coronary reperfusion.

Baseline LV diameters and fractional shortening were similar in the MI and MI-VS groups (Table 3). At 3 days after coronary reperfusion, LV fractional shortening was reduced and LVESD was increased from baseline in both the MI and MI-VS groups to similar degrees. However, further deterioration of LV fractional shortening at 8 weeks after reperfusion observed in MI rabbits was prevented in MI-VS rabbits (Table 3). At 8 weeks after coronary reperfusion, MI-VS rabbits showed significantly smaller LVESD and LVEDD compared with MI rabbits. Data of invasive hemodynamic study are summarized in Table 4. Because 2 rabbits in the MI group with severely depressed LV function (LVEDD >20 mm, LV fractional shortening <14%) developed cardiac arrest during the induction of anesthesia, they were excluded from the invasive hemodynamic study. LV end-diastolic pressure was significantly increased in MI rabbits, which was significantly attenuated in MI-VS rabbits.

LV Passive Pressure-volume Relationship and LV Weight. Plots of ex vivo LV passive pressure-volume relationship are shown in Fig. 4A. A marked difference

Table 3. Changes in Echocardiographic Parameters with Time (Study 2)

	Baseline	3 Days	8 Weeks
LVESD, mm			
MI	7.8 ± 0.2	10.9 ± 0.2†	15.5 ± 0.6†,§
MI-VS	7.9 ± 0.4	9.8 ± 0.5*	11.4 ± 1.1$^{\dagger,\#}$
LVEDD, mm			
MI	13.0 ± 0.3	14.6 ± 0.3	19.2 ± 0.6†,§
MI-VS	12.8 ± 0.3	13.3 ± 0.5	15.5 ± 1.0$^{\dagger,\ddagger,\#}$
FS, %			
MI	39.9 ± 1.3	24.9 ± 1.5†	19.6 ± 1.6†,‡
MI-VS	38.6 ± 1.9	27.1 ± 1.2†	27.2 ± 2.6$^{\dagger,\|\|}$

3 d, 3 days after coronary reperfusion; 8 w, 8 weeks after coronary reperfusion; LVESD, left ventricular (LV) end-systolic diameter; LVEDD, LV end-diastolic diameter; FS, LV fractional shortening.

Data are means ± SEM.

n = 11 in MI group.

n = 10 in MI-VS group.

$^{*}P < .05$.

$^{\dagger}P < .01$ versus baseline.

$^{\ddagger}P < .05$.

$^{\S}P < .01$ versus 3 days.

$^{\|}P < .05$.

$^{\#}P < .01$ versus MI.

Table 4. Invasive Hemodynamic Parameters 8 Weeks after Coronary Reperfusion (Study 2)

	NC	MI	MI-VS
HR, beat/min	335 ± 14	320 ± 5	322 ± 5
MAP, mm Hg	110 ± 3	112 ± 3	112 ± 4
LV dP/dt_{max}, mm Hg/s	4622 ± 234	4546 ± 229	4770 ± 348
LV EDP, mm Hg	4 ± 1	16 ± 3*	7 ± 2†

NC, normal control; HR, heart rate; MAP, mean arterial pressure; LV dP/dt_{max}, the maximum first derivative of left ventricular pressure; LV EDP, left ventricular end-diastolic pressure.
Data are means ± SEM.
n = 7 in NC group, n = 9 in MI group, n = 10 in MI-VS group.
*$P < .01$ versus NC.
†$P < .05$ versus MI.

between NC and MI hearts is evident, whereas the average curve derived from MI-VS hearts is close to that of NC hearts. As shown in Fig. 4B, LV size, indexed by LVV_{10}, of MI-VS hearts was significantly smaller than that of MI hearts ($P < .01$) and reached values close to those of NC hearts. LV weight normalized by body weight increased significantly in both MI and MI-VS hearts compared with NC value (Fig. 4C), but was significantly lower in MI-VS hearts than in MI hearts ($P < .01$).

Histomorphologic Analysis of LV. The risk area sizes were comparable in MI and MI-VS hearts (47 ± 3% vs. 51 ± 5%, P = NS). A transverse LV section demonstrated a smaller LV cavity in the heart receiving VS (Fig. 5A). The LV infarct size was significantly reduced in MI-VS hearts ($P < .05$) compared with MI hearts as shown in Fig. 5B. Because the risk area sizes were comparable in MI and MI-VS hearts, the reduction of infarct size seen in MI-VS rabbits was due to the VS treatment, not insufficient ischemic insults. Wall thickness in LV septum (non-infarct region) was comparable in MI and MI-VS hearts, whereas LV infarct wall thickness was significantly greater in MI-VS hearts than in MI hearts. This resulted in higher thinning ratios in MI-VS hearts than in MI hearts (Fig. 5B). Myocyte hypertrophy in the septum was attenuated in MI-VS hearts as demonstrated by significantly reduced myocyte cross-sectional area compared with MI hearts. Collagen densities in viable myocardial tissue were similar in MI and MI-VS hearts (11 ± 1% versus 9 ± 0%, P = NS).

Plasma MMP. Relative MMP-9 level in plasma was comparable among NC (156 ± 19 A.U., n = 6), MI (147 ± 28 A.U., n = 7), and MI-VS (146 ± 22 A.U., n = 7) groups. Relative MMP-2 level in the MI-VS group (164 ± 20 A.U.) was significantly lower compared with those in the NC (226 ± 17 A.U.) and MI (230 ± 16 A.U.) groups ($P < .05$).

Subgroup Analysis of Effects of VS on LV Remodeling in Large MI. Because the progression of LV remodeling is problematic, especially in patients with large infarct

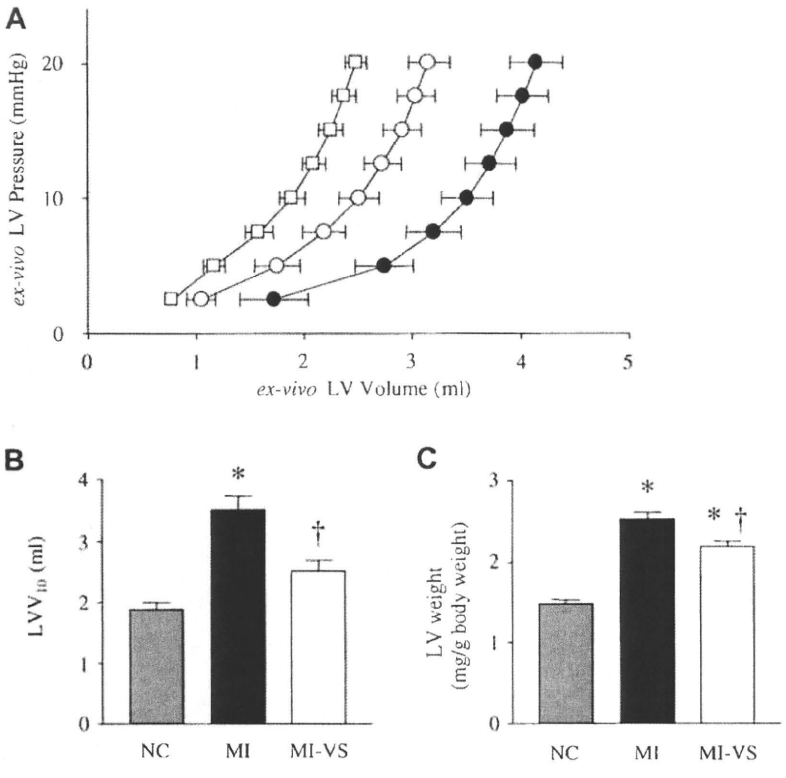

Fig. 4. Ex vivo left ventricular (LV) examinations of normal control (NC) (n = 7), reperfused myocardial infarction (MI) (n = 11), and MI rabbits treated with vagal nerve stimulation (MI-VS) (n = 10) hearts. (A) LV passive pressure-volume relationship in NC (□), MI (●), and MI-VS (○) hearts. (B) Ex vivo LV volume at LV pressure of 10 mm Hg (LVV_{10}). (C) LV weight normalized by body weight. *$P < .01$ versus NC. †$P < .01$ versus MI.

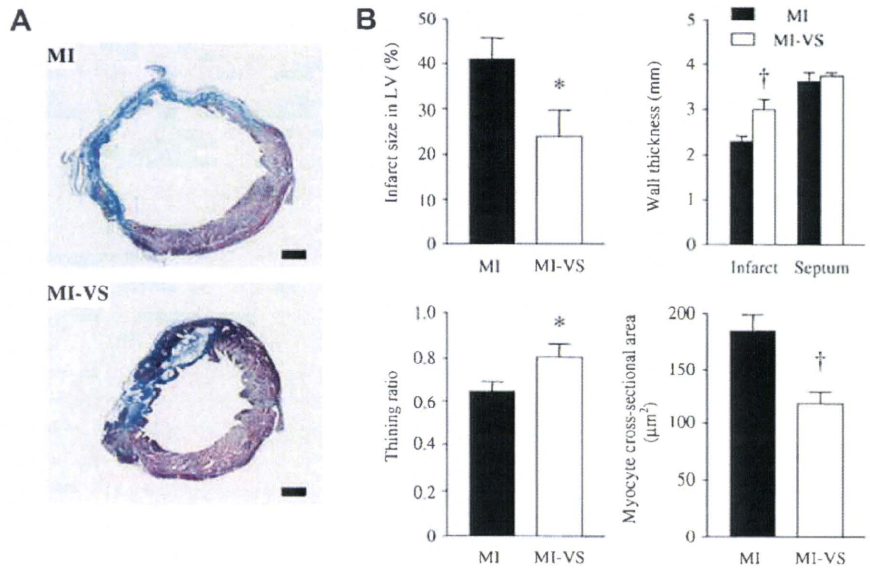

Fig. 5. (A) Transverse LV sections obtained from reperfused myocardial infarction (MI) and MI rabbits treated with vagal nerve stimulation (MI-VS) hearts 8 weeks post-MI. The sections were stained with Masson's trichrome. Blue stained area indicates scared infarct area. Bars = 3 mm. (B) Histomorphometric analyses of LVs in MI (n = 11) and MI-VS (n = 10) hearts. $^{*}P < .05$, $^{\dagger}P < .01$ versus MI.

size,[1] we evaluated the effects of VS on the parameters of LV remodeling (LV weight and LVEDD at 8 weeks after coronary reperfusion) in animals with large infarct size (>30% of LV, 8 MI. and 4 MI-VS rabbits). LV infarct size was comparable in MI and MI-VS hearts (49 ± 3% versus 44 ± 6%, P = NS). However, LV weight was significantly lower in MI-VS hearts than in MI hearts (2.2 ± 0.1 versus 2.6 ± 0.1 mg/g body weight, $P < .05$). There was a strong trend of reduction in LVEDD in MI-VS hearts compared with MI hearts, although the difference did not reach statistical significance (15.1 ± 2.0 versus 18.9 ± 0.8 mm, $P = .052$).

Discussion

The major new findings of the present study were as follows. In the acute inflammatory phase of reperfused MI, VS decreased TNF-α protein level and suppressed neutrophil infiltration in the infarcted myocardium. In the chronic phase of reperfused MI, VS markedly attenuated LV dysfunction and remodeling, even though VS was limited to a short period early after MI. Although several acute experimental studies examined the cardioprotective effects of VS in reperfused MI, they lacked detailed assessment of LV function and structure as done in this study.[5–7]

Cardioprotective Effects of VS and Cytokine Expressions

The beneficial effects of VS on reperfused MI are primarily attributable to the reduction of infarct size.[1,21] Several cardioprotective mechanisms of VS in ischemic myocardium have been reported previously. In a neutrophil-free isolated heart preparation, VS attenuated ischemia-reperfusion injury by protecting the myocytic mitochondria.[5] In a non-reperfused MI model, VS protected cardiomyocytes by upregulating hypoxia-inducible factor-1α pathway, and reduced infarct size.[22] Acetylcholine, the principal vagal neurotransmitter, mediated these direct protective effects on cardiomyocyte through the muscarinic acetylcholine receptor pathway.[5,22] These mechanisms may have contributed to the reduction of infarct size by VS in the present study. In addition, suppression of myocardial neutrophil infiltration in acute MI phase might also contribute to the reduction of infarct size by VS. Although reperfusion of the ischemic myocardium is necessary to salvage viable myocytes from eventual death, reperfusion also causes tissue damage.[9] Reperfusion injury in the acute phase of MI shares many characteristics with inflammatory reactions. Neutrophils feature prominently in this inflammatory reaction.[9] It is well known that in the reperfused ischemic myocardium, upregulated TNF-α accelerates the infiltration of neutrophils.[8,23] In this study, VS suppressed neutrophil infiltration into the infarcted myocardium possibly through inhibition of TNF-α expression, which might suppress the neutrophil-induced myocyte injury, thereby reducing the infarct size. Acetylcholine attenuates the release of TNF-α from macrophages through the nicotinic acetylcholine receptor pathway.[10,11] Cardiac mast cell is an important source of TNF-α in ischemic myocardium,[23] and expresses the nicotinic receptor.[24] In our model, VS might have directly reduced TNF-α expression on cardiac mast cells via the nicotinic acetylcholine receptor pathway.

Myocardial IL-1β protein content was not changed in our MI model. Previous experimental study also reported

similar results and suggested an insignificant role of IL-1β as an upstream inducer of post-reperfusion inflammatory reactions.[23] Myocardial IL-6 protein expression was not affected by VS in this study. Previous clinical study indicated that VS decreased plasma IL-6 concentration in patients with advanced heart failure, but the reduction was transient and noted only at 3 months after commencing VS.[4] Although the increase in plasma IL-6 has been associated with progression of LV contractile dysfunction in patients with heart failure, recent experimental research suggests that IL-6 expression in viable myocardium may play a pivotal role in cytoprotection.[25] Several biochemical and hemodynamic factors have been shown to regulate IL-6 expression after MI. IL-6 mRNA expression in mononuclear cells infiltrating the infarcted myocardium is upregulated by TNF-α.[23] Gwechenberger et al[16] have shown the reperfusion-dependent expression of IL-6 mRNA in cardiomyocytes in the viable border zone. Perfusion dependency of IL-6 expression was also observed in patients with reperfused MI, where plasma IL-6 concentration positively correlated with ischemic myocardial collateral flow.[26] In the present study, VS-induced TNF-α reduction might have decreased myocardial IL-6 expression. On the other hand, the beneficial effect of VS on myocardial perfusion[27] or the direct cardiomyocyte-protecting effect of VS[5] might have increased de novo synthesis of IL-6 in the jeopardized but viable myocardium. In VS, all these factors may operate simultaneously.

Myocardial CRP expression increased drastically after MI, which was not affected by VS in this study. After MI, CRP is produced from the liver partly as a response to stimulation by IL-6 released from the damaged heart.[28] Because we found that cardiac expression of IL-6 was similar in the MI and MI-VS groups, it is reasonable that myocardial CRP content was not different between the 2 groups in the present experiment. CRP-mediated complement activation in the myocardium was associated with increase in infarct size and LV remodeling after MI in several experimental and clinical studies,[28,29] although this association remains controversial.[30,31]

Our previous studies suggest that bradycardia plays a significant role in cardioprotection by VS.[3] However, the present results indicate that the cardioprotective effect of VS does not necessarily require strong bradycardia. Huston et al demonstrated that in a mouse model of sepsis, mild intensity of VS drastically reduces serum TNF-α without inducing bradycardia.[11] Furthermore, the cardioprotective effect of VS through protecting myocytic mitochondria is also independent of the degree of bradycardia.[5] Increasing VS intensity to attain strong bradycardia can cause unwanted side effects such as local pain in animals and also in patients.[3,4] Although the degree of bradycardia has been the primary parameter used in adjusting the intensity of VS,[4] additional parameters may be required for deciding the proper therapeutic strategy of VS in clinical application.

MMP Inhibition and LV Remodeling. Subgroup analysis of study 2 demonstrated that VS attenuated LV hypertrophy when comparing MI and MI-VS hearts with similarly large infarct size. This finding indicates that VS indeed confers an antiremodeling effect beyond that through reduction in infarct size. Reduction of MMP-9 activity in the infarcted myocardium early after MI may contribute to this antiremodeling effect of VS.[18,32–34] In addition to the loss of contractile cardiomyocytes, pathological degradation and reconstitution of extracellular matrix contribute to the progression of LV remodeling after MI, where MMP and TIMP play crucial roles. After MI, pharmacological MMP inhibition attenuated LV remodeling without affecting infarct size even if given for a short period.[18,33] Suppression of the infiltration of neutrophil, an important source of MMP-9 after myocardial ischemia reperfusion,[32] may be one reason of the reduction of MMP-9 contents by VS in infarct observed in this study. VS did not change the collagen content of the viable myocardium at 8 weeks after MI in spite of reduced MMP-9 expression early after MI. Several studies also reported that MMP inhibition improved LV remodeling without changing the collagen contents within the infarcts or in viable tissues after MI.[18,33] Lindsey et al demonstrated in a rabbit model of MI that inhibition of MMP activities attenuated LV dilatation and preserved the infarct wall thickness and the thinning ratio without changing the tissue collagen content.[33] Their findings are almost compatible to the present results. These observations suggest that a noncollagenolytic mechanism may also play a critical role in regulating LV remodeling. Plasma MMP-9 concentration measured 8 weeks after MI was not reduced in MI-VS rabbits compared with MI rabbits and controls. This indicates that the MMP-9 suppressive effect of VS delivered early after MI did not last long. This might be beneficial in terms of LV remodeling. A previous experimental study[34] demonstrated that MMP inhibition early after MI conferred beneficial effects on LV remodeling, but chronic prolonged MMP inhibition was associated with adverse effects on LV remodeling. MMP-8, a neutrophil collagenase, has been shown to increase in cardiac tissue after MI and relate to LV rupture in MI patients.[35] In this study, suppression of neutrophil infiltration is probably the primary reason for the reduction of myocardial MMP-8 contents by VS.

MMP-1 is mainly produced by cardiac fibroblasts. MMP-2 is mainly expressed in cardiomyocytes after ischemic injury.[35] MMP-7 is expressed in macrophages and cardiomyocytes after MI.[36] After reperfused MI, myocardial protein contents of MMP-1, -2, and -7 were not affected by VS. Taken together, VS appears to specifically affect neutrophil-associated MMPs.

Myocardial TIMP-1 protein level was not affected by VS in this study, which seems inconsistent with our previous finding.[12] TIMP-1 level increased drastically after 24 hours of coronary reperfusion in the present study (>1200 ng/g protein, compared with that observed after 3 hours of reperfusion in rabbits in our previous study (<500 ng/g protein).[12] On the other hand, the intensity of VS in this study was rather mild compared with that in the previous